

Chunk-Boundary Artifact in Action-Chunked Generative Policies: A Noise-Sensitive Failure Mechanism

Rui Wang¹

Abstract

Action chunking has become a central design choice for generative visuomotor policies, yet the execution discontinuities that arise at chunk boundaries remain poorly understood. In a frozen pretrained action-chunked policy, we identify **chunk-boundary artifact** as a **noise-sensitive failure mechanism**. First, artifact is strongly associated with task failure ($p < 10^{-4}$, permutation test) and emerges during the rollout rather than only as a post-hoc symptom. Second, under a fixed observation context, changing only latent noise systematically modulates artifact magnitude. Third, by identifying artifact-related directions in noise space and applying trajectory-level steering, we reliably alter artifact magnitude across all evaluated tasks. In hard-task settings with remaining outcome headroom, the success/failure distribution shifts accordingly; on near-ceiling tasks, positive gains are compressed by policy saturation, while the negative causal effect remains visible. Overall, we recast boundary discontinuity from an unavoidable execution nuisance into an analyzable, noise-dominated, and intervenable failure mechanism.

1 Introduction

Action chunking—predicting and executing a short sequence of future actions in a single forward pass—has become a key design choice in generative robot policies [2, 3, 1]. By amortizing computation across multiple timesteps, chunked policies achieve lower latency and smoother behavior within each chunk. However, at the *boundary* where one chunk ends and the next begins, the policy must replan from a new observation context, often producing visible discontinuities in the executed action trajectory.

Prior work has recognized such boundary artifacts and proposed several execution-time remedies, including temporal ensembling [3], learned continuation models [7], and real-time re-execution controllers [10, 11]. These methods largely treat artifact as an unavoidable execution-layer issue to be smoothed *after the fact*. A natural but under-explored question is therefore: *what determines the severity of chunk-boundary artifact, and can it be changed before execution rather than only repaired afterward?*

We study chunk-boundary artifact in a frozen pretrained flow-matching policy, OpenPI [1], and establish three findings. Concretely, we use two frozen OpenPI checkpoints in the experiments: `pi0.5-libero` and `pi0-libero`.

¹Nanjing University

1. **Artifact** \leftrightarrow **outcome**. Failed episodes exhibit substantially stronger boundary artifact than successful ones (boundary-gap difference +0.238, $p < 10^{-4}$). Control analyses with matched horizons and contact-free windows show that this separation already emerges before terminal contact events, positioning artifact as a *failure mechanism* rather than a mere consequence of failure.
2. **Noise** \rightarrow **artifact**. Under a fixed observation context, changing only the latent noise \mathbf{z} fed into the generator is sufficient to systematically modulate artifact magnitude. In a fixed-context scan with 384 samples, the mean cross-context standard deviation of the boundary–interior jerk contrast is 0.040. A decomposition over current-chunk noise \mathbf{z}_0 and next-chunk noise \mathbf{z}_1 confirms that both contribute, consistent with the intuition that artifact depends on the *transition* between consecutive chunks.
3. **Steering** \rightarrow **artifact** \rightarrow **outcome**. The noise–artifact map has directional structure: under fixed contexts, we identify local noise directions and perform one-dimensional α sweeps along them, yielding an average correlation of $r = 0.97$ between steering strength α and the first-boundary jerk contrast. In full-trajectory steering experiments, *targeted-good* and *targeted-bad* interventions with equal magnitude and opposite sign reliably decrease or increase the episode-level boundary–interior jerk contrast. On near-ceiling tasks, this mechanism change does not necessarily translate into additional success-rate gains; on hard tasks with remaining headroom, however, it shifts the outcome distribution in the corresponding direction.

Together, these results recast chunk-boundary artifact from a generic execution nuisance into an analyzable, *noise-dominated and intervenable failure mechanism* that can be manipulated without retraining the base policy.

2 Preliminaries

2.1 Action-chunked generative policy

We consider a visuomotor policy π_θ that, given an observation context \mathbf{x}_t at time t , generates a future action chunk

$$\mathbf{a}_{t:t+H} = \pi_\theta(\mathbf{x}_t, \mathbf{z}), \quad (1)$$

where $\mathbf{z} \sim \mathcal{N}(0, I)$ is the latent noise variable of the generative model (e.g., the initial noise of a diffusion or flow-matching process).

At deployment time, the agent executes only the first $K \leq H$ actions of each chunk and then replans from the new context \mathbf{x}_{t+K} . This creates a periodic chunk-boundary structure at timesteps $t, t+K, t+2K, \dots$

2.2 Boundary artifact

At each boundary, the policy transitions from the tail of the previous chunk to the head of the next chunk. Because consecutive chunks are generated independently from different

contexts and noise samples, discontinuities can arise at the boundary. We quantify this using the *boundary–interior jerk contrast*

$$J_{\text{contrast}} = \frac{1}{|\mathcal{B}|} \sum_{p \in \mathcal{B}} \bar{j}_p - \frac{1}{|\mathcal{I}|} \sum_{p \in \mathcal{I}} \bar{j}_p, \quad (2)$$

where $j_t = \|\mathbf{a}_t - 2\mathbf{a}_{t-1} + \mathbf{a}_{t-2}\|_2$ is the action jerk, $p(t) = t \bmod K$ is the phase within the replanning cycle, $\mathcal{B} = \{0, 1\}$ denotes boundary phases, $\mathcal{I} = \{2, 3, 4\}$ denotes interior phases, and \bar{j}_p is the mean jerk at phase p over a rollout. We also measure *boundary transition jerk*, defined as the L_2 norm of the second finite difference at the boundary.

The *episode-level boundary–interior jerk contrast* is the rollout-level version of this statistic and summarizes the excess discontinuity at boundary phases relative to interior phases.

2.3 Questions addressed in this paper

We study the following questions in a *frozen* pretrained policy, i.e., without updating policy weights:

1. Is boundary artifact associated with task outcome, and if so, is it a plausible failure mechanism?
2. Does latent noise causally influence artifact magnitude?
3. Can directional noise steering change artifact and thereby alter the outcome distribution?

3 Boundary Artifact and Task Outcome

3.1 Experimental setup

We evaluate a pretrained OpenPI policy on two Goal tasks from the LIBERO benchmark [6]: *goal 0* (“open the middle drawer of the cabinet”) and *goal 3* (“open the top drawer and put the bowl inside”). Each task is evaluated over 70 rollout episodes, with replanning every $K = 5$ executed steps and an action horizon of $H = 10$. For each episode we record the full action trajectory and compute the episode-level boundary–interior jerk contrast together with phase-resolved jerk profiles.

3.2 Results

Table 1 shows that failed episodes exhibit substantially larger boundary–interior jerk contrasts on both tasks. Crucially, this separation persists under two control conditions: **contact-free** windows, which exclude timesteps near object contact, and **contact-free first 50 steps**, which isolates early trajectory segments before any terminal contact event. The group difference in this contrast already appears in early contact-free portions of the trajectory, arguing against the explanation that high artifact is merely a late-stage consequence of failure. In addition, after truncating success and failure rollouts to the same matched horizon, the boundary-aligned action-jerk pulses remain visible, showing that the effect is not simply induced by episode-length differences, as shown in fig. 1.

Table 1: Comparison of the episode-level boundary–interior jerk contrast between successful and failed episodes. “Success mean” and “Failure mean” denote the within-group means of this metric. All p values are from 20,000-sample permutation tests.

Task	Control condition	Success mean	Failure mean	Δ	p value
goal 3	All episodes	0.102	0.341	+0.238	$< 10^{-4}$
	Contact-free	0.100	0.297	+0.197	$< 10^{-4}$
	Contact-free first 50 steps	0.093	0.138	+0.045	0.005
goal 0	All episodes	0.108	0.219	+0.110	$< 10^{-4}$
	Contact-free	0.108	0.185	+0.077	0.002
	Contact-free first 50 steps	0.049	0.070	+0.021	0.008

From the time-course perspective, failure trajectories show stronger action-jerk pulses around each replanning boundary, consistent with our phase-locked aggregation: artifact is concentrated at boundary phases (0/1) of the 5-step replanning cycle and is stronger in failed episodes.

Interpretation. We do not claim that boundary artifact is the only cause of failure. However, its temporal precedence, persistence under the control windows above, and the later intervention results (section 5) support a stronger reading: boundary artifact is a *plausible failure mechanism*—a causal contributor to failure risk rather than a post-hoc symptom.

4 Latent Noise Modulates Boundary Artifact

4.1 Fixed-context noise scan

To isolate the effect of latent noise on artifact, we fix the observation context \mathbf{x} and vary only the chunk noise \mathbf{z} . Concretely, we collect 16 observation contexts from goal 3 rollouts and sample 24 independent noise realizations per context, yielding $16 \times 24 = 384$ action chunks. For each sample we measure boundary transition jerk and the local boundary–interior jerk contrast.

The results confirm that changing noise alone is sufficient to modulate artifact: the mean cross-context standard deviation of the boundary–interior jerk contrast is $\sigma = 0.040$ (95% bootstrap CI [0.030, 0.052]), and the corresponding value for boundary transition jerk is $\sigma = 0.038$ (95% bootstrap CI [0.028, 0.048]); the maximum context-level standard deviations reach 0.097 and 0.084, respectively. This indicates that artifact variability is not driven solely by observation differences; it contains a substantial noise-dominated component, as shown in fig. 2.

4.2 Noise decomposition: \mathbf{z}_0 and \mathbf{z}_1

Because boundary artifact depends on the transition between two consecutive chunks, both the current-chunk noise \mathbf{z}_0 and the next-chunk noise \mathbf{z}_1 may contribute. We therefore perform a controlled decomposition in which, for each of two contexts, we vary only \mathbf{z}_0 , only \mathbf{z}_1 , or both (5 samples per condition).

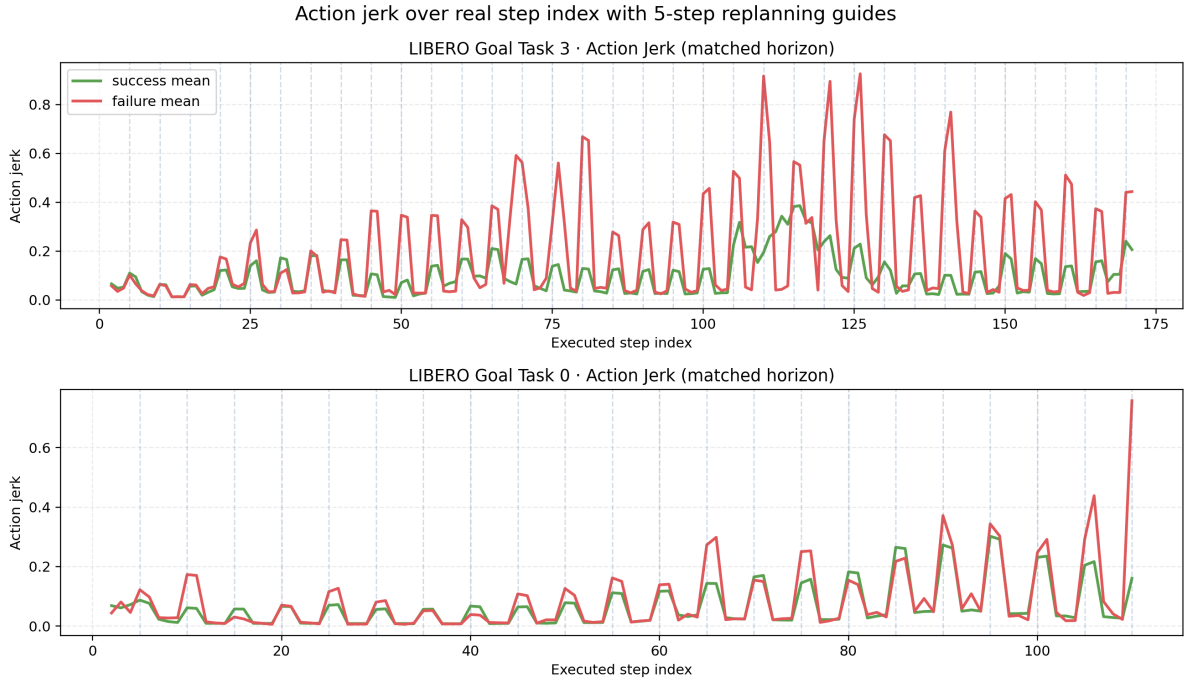


Figure 1: Matched-horizon action-jerk time courses after truncating success and failure rollouts to a common comparable length. Even under matched horizon, failure trajectories still show stronger jerk pulses around each replanning boundary, indicating that the phenomenon is not driven purely by episode-length differences. Vertical dashed lines mark replanning boundaries every 5 steps.

Table 2 shows that both \mathbf{z}_0 and \mathbf{z}_1 make substantial contributions to artifact variation. For goal 3, the contribution of \mathbf{z}_1 is slightly larger than that of \mathbf{z}_0 , consistent with the intuition that boundary artifact depends strongly on the content generated for the *next* chunk. The “vary both” condition is not a simple additive combination of the individual variances, indicating nonlinear interaction between the two noise sources at the boundary rather than independent superposition.

We also repeat the same decomposition on the harder LIBERO-10 task 8 (4 contexts, 8 samples per condition). That replication again shows that both \mathbf{z}_0 and \mathbf{z}_1 affect first-boundary artifact, but their relative strengths are not fixed: on task 8, \mathbf{z}_0 is slightly stronger than \mathbf{z}_1 . The more robust cross-task conclusion is therefore not that “ \mathbf{z}_1 always dominates,” but rather that *chunk noise on both sides of the boundary matters, and the dominant term depends on task and context.*

The first boundary as a clean probe. We focus on the *first* chunk boundary because later boundaries are contaminated by accumulated state drift, contact events, and compounding replanning errors. The first boundary provides the cleanest window for isolating the $\mathbf{z} \rightarrow \mathcal{A}$ mechanism. This is an experimental design choice, not a claim that only early noise matters.

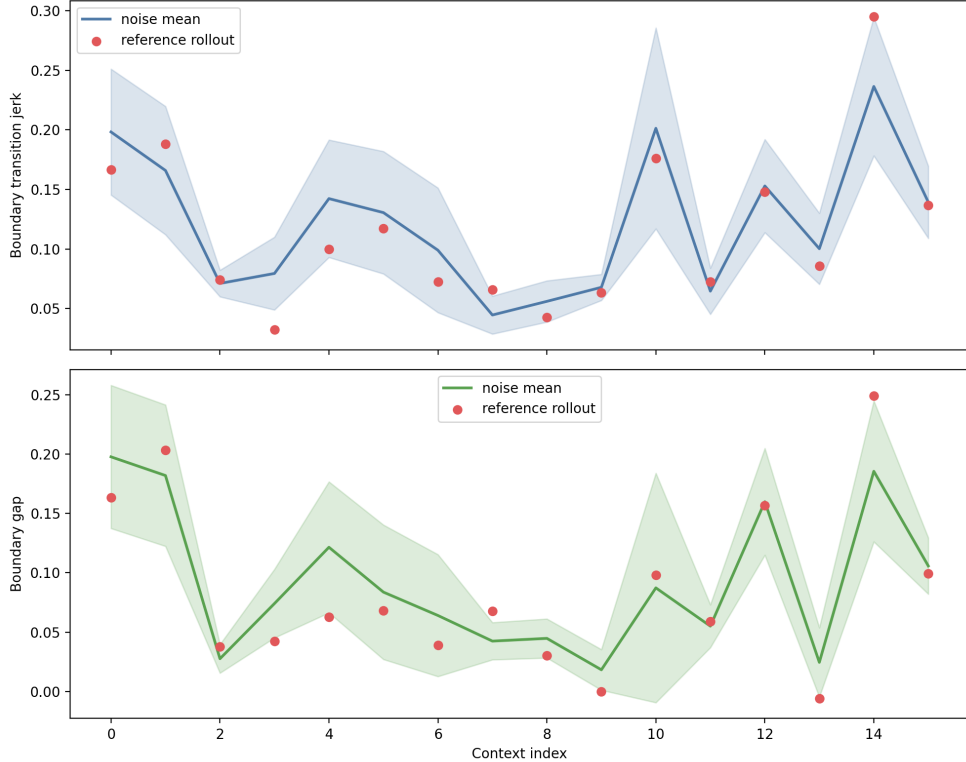


Figure 2: Artifact variation when the observation context is fixed and only the latent noise is changed. Shaded regions indicate the mean \pm standard deviation across noise samples under the same context, and red dots denote reference rollouts. Top: boundary transition jerk. Bottom: local boundary–interior jerk contrast.

5 Directional Steering Reveals an Intervenable Failure Mechanism

5.1 Identifying artifact-related directions in noise space

Since noise modulates artifact, we next ask whether this dependence has exploitable *directional* structure. For each observation context, we search for a perturbation direction \mathbf{d} in noise space such that steering

$$\mathbf{z}' = \mathbf{z} + \alpha \mathbf{d} \quad (3)$$

produces monotonic changes in artifact as α varies.

Specifically, for 4 contexts from LIBERO-10 task 8 (“put both moka pots on the stove”), we sample 12 random directions in noise space ($\epsilon = 0.5$), select the direction \mathbf{d}^* that maximizes the absolute artifact difference between positive and negative steering extremes, and then scan $\alpha \in \{-1, -0.5, -0.25, 0, 0.25, 0.5, 1\}$.

5.2 Controllability results

The selected local directions exert strong monotonic control over artifact: within each fixed context, a one-dimensional α sweep along the chosen direction yields a mean Pearson correlation of $r = 0.904$ with boundary transition jerk and $r = 0.968$ with the

Table 2: Noise decomposition: standard deviation of first-boundary artifact metrics under different noise-variation conditions. BTJ = boundary transition jerk.

Task	Condition	BTJ std	Gap std
goal 3	Vary \mathbf{z}_0 only	0.029	0.030
	Vary \mathbf{z}_1 only	0.035	0.040
	Vary both	0.038	0.038
goal 0	Vary \mathbf{z}_0 only	0.022	0.020
	Vary \mathbf{z}_1 only	0.024	0.025
	Vary both	0.017	0.019

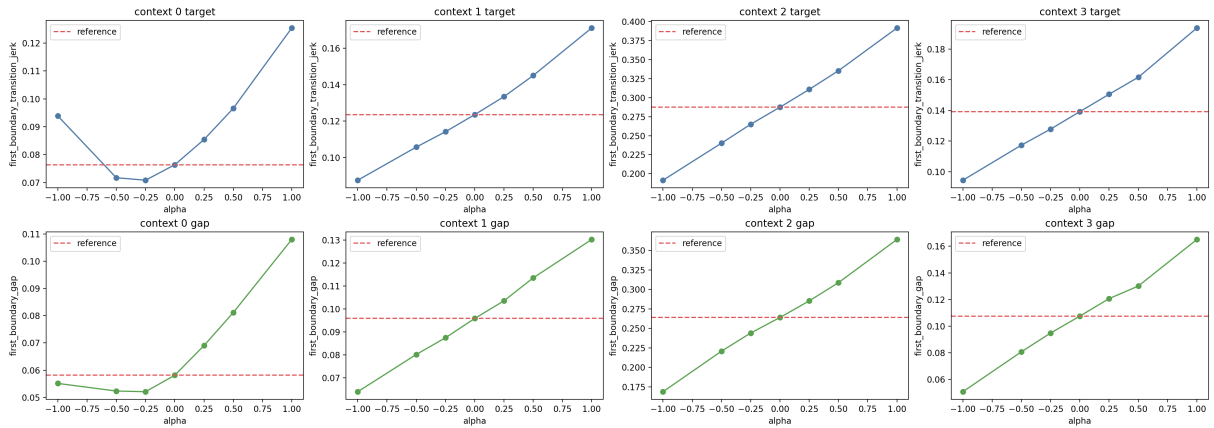


Figure 3: Artifact-related directions identified on LIBERO-10 task 8. Across 4 contexts, the target artifact metric and the first-boundary jerk contrast vary nearly monotonically with steering strength α , indicating that artifact can be stably controlled along specific directions in noise space.

first-boundary jerk contrast. The mean artifact range induced across the α scan is 0.108, comparable to the failure–success group difference observed in section 3. This confirms that steering in noise space can produce artifact changes of practically meaningful magnitude, as shown in fig. 3. However, this directional result should be understood as evidence of *local controllability*, rather than as a global linear control law. Mild nonlinear deviations remain visible at larger $|\alpha|$, suggesting that stronger steering can move the response outside the local linear regime and progressively away from noise regions more commonly visited during training and standard sampling. Our exploratory high-strength trials are consistent with this interpretation: when steering strength is pushed well beyond the main experimental setting, policy performance begins to deteriorate, indicating that this steering mechanism remains stable only within a finite operating range.

5.3 Trajectory-level steering: ceiling and non-ceiling settings

To move beyond the earlier prefix pilot and test a more stable deployment scenario, we switch to *trajectory-level steering*: once sufficient boundary history is available, each subsequent replanning step applies equal-magnitude positive or negative steering along the same artifact-related direction. We previously tried perturbing only early noise and then bridging final success/failure from the first-boundary metric, but the resulting signal

Table 3: Summary of trajectory-level steering. The first row is the LIBERO-10 ceiling task and the second row is the LIBERO-10 non-ceiling task. The three intervention groups use equal-magnitude steering in opposite directions.

Task group	Success rate			Episode boundary–interior jerk contrast		
	Baseline	Good	Bad	Baseline	Good	Bad
LIBERO-10 ceiling	1.000	1.000	0.762	0.171	0.081	0.381
LIBERO-10 non-ceiling	0.674	0.791	0.535	0.090	0.055	0.177

was weak. We therefore turn directly to sustained trajectory-level steering and test whether continuous intervention can more stably control artifact and shift the outcome distribution when task headroom remains.

We first perform full-trajectory steering screening across the entire LIBERO-10 suite and then organize the evidence into two regimes: (1) **ceiling-like tasks**, where the base policy is already near the success-rate ceiling, and (2) **non-ceiling tasks**, where success remains meaningfully improvable. The non-ceiling result reported in the main text comes from a multi-seed aggregation on task 8, whereas the ceiling-like result is used to illustrate representative phenomenology in near-saturated settings.

Table 3 together with Figure 4 supports three robust conclusions; a broader aggregate over the full set of trajectory-level experiments is shown in Appendix Figure A1. First, **the change in artifact magnitude is consistently visible in all settings**: for both ceiling and non-ceiling tasks, *targeted-good* systematically suppresses the episode-level boundary–interior jerk contrast, while *targeted-bad* increases it. This shows that boundary artifact is not merely a passive observational phenomenon; it is a mechanism state that can be reliably controlled by noise steering.

Second, **the good and bad directions are direction-specific rather than generic perturbation effects**. The three groups use equal-magnitude interventions, yet opposite steering directions produce a stable ordering of $good < baseline < bad$ in boundary–interior jerk contrast. Hence the effect is not simply “adding more noise” but acting along a specific direction tied to boundary artifact.

Third, **whether the outcome distribution moves depends on whether the policy still has headroom**. On the LIBERO-10 ceiling task, the baseline and targeted-good conditions both remain at 1.0 success rate, indicating that the benefit of positive steering is compressed by the ceiling effect. Yet targeted-bad already drops to 0.762, while the boundary–interior jerk contrast still preserves the strong ordering $good < baseline < bad$; thus even when upward gains are saturated, the negative causal effect remains visible.

By contrast, on the LIBERO-10 non-ceiling task, the mechanism change is further translated into an outcome shift: *targeted-good* both lowers the boundary–interior jerk contrast and raises success to 0.791, whereas *targeted-bad* lowers success to 0.535. This non-ceiling conclusion is not driven by one specific seed; it is supported by a multi-seed aggregation on task 8 with 43 rollouts per group. It is therefore better interpreted as a stable pattern in a hard-task regime with remaining headroom, rather than as a chance uplift from a local seed configuration. In particular, bad-direction intervention consistently suppresses success on the non-ceiling task, supporting a stronger interpretation than “artifact is one factor among many failures.” Conversely, when the baseline success rate is already very low for a seed or context, the policy is closer to a failure floor. In

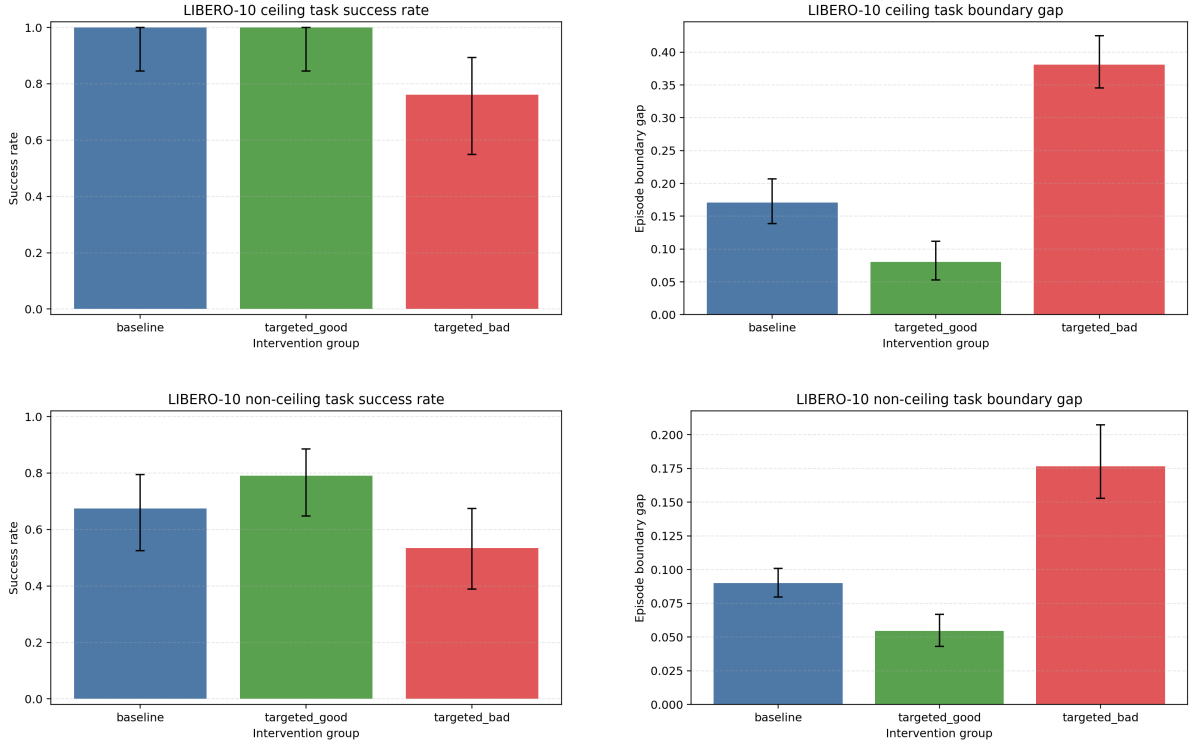


Figure 4: Summary of trajectory-level steering. The top row shows the LIBERO-10 ceiling task and the bottom row shows the LIBERO-10 non-ceiling task. Error bars denote 95% confidence intervals: Wilson CIs for success rate and bootstrap CIs for episode boundary–interior jerk contrast. In both settings, targeted-good consistently lowers the boundary–interior jerk contrast and targeted-bad consistently raises it; clear separation in success rate mainly appears in the non-ceiling hard-task setting.

that regime, steering may still change artifact magnitude, but the visible response in success rate can be strongly compressed, making clear separation in pooled statistics harder to obtain. This further suggests that our method is best understood as an auxiliary mechanistic intervention that is effective when outcome headroom exists, rather than as a universal solution that reliably improves performance under all initial conditions. Rather, boundary artifact is a **noise-dominated failure mechanism that can be directionally amplified or suppressed**.

6 Related Work

Action chunking and boundary discontinuity. ACT [3] introduces temporal ensembling to smooth boundary transitions. RTC [10] and REMAC [11] further demonstrate that chunk-boundary discontinuity is a real execution problem and propose controller-level fixes. More recent work [7] models cross-chunk continuation during training. Bidirectional Decoding (BID) [8] further mitigates boundary discontinuity in closed-loop execution through test-time cross-chunk coherence-based selection. Diffusion Forcing [9] weakens the fixed chunk-boundary issue from a different training paradigm by allowing different noise levels across timesteps. Our approach differs in that we neither modify execution nor retrain the policy; instead, we analyze the mechanism that produces artifact and intervene in the latent space of a frozen policy.

Initial noise optimization in generative models. InitNO [12] shows that systematically optimizing the initial noise of diffusion-based image generators can improve output quality. This provides cross-domain motivation for our work: if initial noise matters for visual sample quality, it may also influence execution quality in generative robot policies. Related work such as NoiseCLR [5] further suggests that diffusion noise space itself can contain interpretable directional structure. However, InitNO and NoiseCLR focus on image semantics or generation quality, whereas we target a specific control-side mechanism: chunk-boundary artifact.

Latent-space policy improvement. DSRL [13] optimizes a generative policy in latent noise space with a learned reward model, without retraining the base policy. We adopt the broader idea that latent space can serve as an effective intervention surface, but our core contribution is the identification of the boundary-artifact mechanism itself rather than a new reward or optimization algorithm.

7 Discussion and Limitations

What we can and cannot claim. Our evidence supports a specific claim: boundary artifact is a *noise-dominated and intervenable failure mechanism*. Intervention reliably changes artifact magnitude and, when task headroom exists, shifts the success/failure distribution. We do *not* claim that artifact is the sole cause of failure, nor that positive steering must linearly improve success on every task. A more accurate reading of the current results is that mechanism-level control is stable across tasks, whereas outcome-level gains can be compressed by policy saturation and ceiling effects.

Scalability of direction search. Our current direction search is based on random sampling followed by selection. More sophisticated optimization—for example, gradient-based search through the denoiser—may find better directions and support higher-dimensional interventions.

Online overhead. The main extra cost in the current implementation comes not from noise sampling itself but from local direction search at each replanning boundary. This step requires several additional policy forwards over candidate directions, so the present method should not be framed as a low-overhead real-time module. That said, it does not require extra environment interaction, online training, or an external reward model. For real-time deployment, a more natural next step would be to distill the local search into a context-conditioned direction predictor.

Structured information in noise space. Our results further suggest that the noise space of a robot policy may contain low-dimensional structure related to execution quality. On task 8, within fixed-context directional scans, sweeping α along a selected local steering direction produces nearly monotonic changes in the first-boundary jerk contrast, with average correlation $r = 0.97$. This resonates with observations from image generation that noise or latent spaces contain interpretable directions [4, 5]; here, however, the attribute is not age or pose but action-transition continuity itself. A natural next step is

to apply PCA or more general subspace analysis to the noise space and test whether leading components also explain execution-quality indicators beyond the boundary–interior jerk contrast, such as pre-contact jerk, end-effector stability, or late-stage control margin.

8 Conclusion

In a frozen pretrained action-chunked generative policy, we identify chunk-boundary artifact as a noise-sensitive failure mechanism. Three lines of evidence support this characterization: (1) boundary artifact is strongly associated with failure and appears during the episode as a plausible causal contributor; (2) latent noise systematically modulates artifact magnitude under fixed observation contexts; and (3) directional noise steering stably changes artifact magnitude across tasks and further shifts outcome distributions on hard tasks with remaining headroom.

These findings recast boundary discontinuity from an unavoidable execution nuisance into an analyzable failure mechanism with a clear intervention surface. Rather than only repairing artifact after it appears or retraining the base policy, we show that chunk-transition quality is determined in part by latent noise space itself—and can be systematically improved or degraded there.

References

- [1] K. Black, N. Brown, D. Driess, A. Escontrela, M. Nasiriany, et al. π_0 : A vision-language-action flow model for general robot control. In *RSS*, 2025.
- [2] C. Chi, Z. Xu, S. Feng, Y. Du, E. Cousineau, et al. Diffusion Policy: Visuomotor Policy Learning via Action Diffusion. In *RSS*, 2023.
- [3] T. Z. Zhao, V. Kumar, S. Levine, and C. Finn. Learning Fine-Grained Bimanual Manipulation with Low-Cost Hardware. In *RSS*, 2023.
- [4] R. Haas, I. Huberman-Spiegelglas, R. Mulayoff, S. Graßhof, S. S. Brandt, and T. Michaeli. Discovering Interpretable Directions in the Semantic Latent Space of Diffusion Models. In *IEEE International Conference on Automatic Face and Gesture Recognition (FG)*, 2024.
- [5] Y. Dalva and P. Yanardag. NoiseCLR: A Contrastive Learning Approach for Un-supervised Discovery of Interpretable Directions in Diffusion Models. In *CVPR*, 2024.
- [6] B. Liu, Y. Zhu, C. Gao, Y. Feng, Q. Liu, et al. LIBERO: Benchmarking Knowledge Transfer for Lifelong Robot Learning. In *NeurIPS Datasets and Benchmarks*, 2023.
- [7] Y. Liu, H. Yu, J. Zhao, B. Li, D. Zhang, M. Li, et al. Learning Native Continuation for Action Chunking Flow Policies. *arXiv preprint arXiv:2602.12978*, 2026.
- [8] Y. Liu, J. I. Hamid, A. Xie, Y. Lee, M. Du, and C. Finn. Bidirectional Decoding: Improving Action Chunking via Closed-Loop Resampling. In *ICLR*, 2025.

- [9] B. Chen, D. Martí Monsó, Y. Du, M. Simchowitz, R. Tedrake, and V. Sitzmann. Diffusion Forcing: Next-token Prediction Meets Full-Sequence Diffusion. In *NeurIPS*, 2024.
- [10] K. Black, M. Y. Galliker, and S. Levine. Real-Time Execution of Action Chunking Flow Policies. In *NeurIPS*, 2025.
- [11] H. Wang, G. Zhang, Y. Yan, Y. Shang, R. R. Kompella, and G. Liu. Real-Time Robot Execution with Masked Action Chunking. In *ICLR*, 2026.
- [12] X. Guo, J. Liu, M. Cui, J. Li, H. Yang, and D. Huang. InitNO: Boosting Text-to-Image Diffusion Models via Initial Noise Optimization. In *CVPR*, 2024.
- [13] A. Wagenmaker, M. Nakamoto, Y. Zhang, S. Park, W. Yagoub, et al. Steering Your Diffusion Policy with Latent-Space Reinforcement Learning. In *CoRL*, 2025.

Appendix

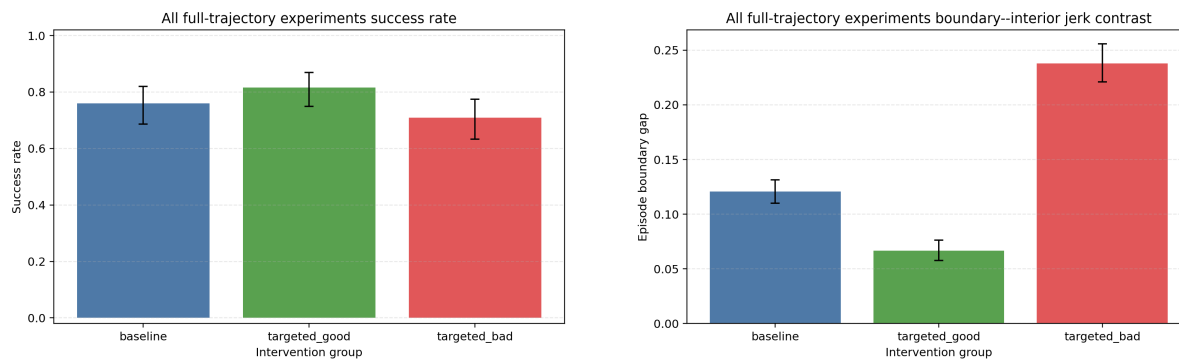


Figure A1: Aggregate over the full set of full-trajectory steering experiments included here ($n = 158$ per group). Left: success rate. Right: episode boundary–interior jerk contrast. The pool includes ceiling-like, non-ceiling, failure-floor, and one-off settings whose outcome-level interpretation remains uncertain; accordingly, success-rate separation is compressed, while the directional ordering of the mechanistic metric remains visible.